Supporting Information

Yi and Wagner 10.1073/pnas.1717910115

SI Materials and Methods

Reagents and Antibodies. EGFP-hPMCA2z/b (no. 47584) and mCherry–β-actin (no. 54967) plasmids were ordered from Addgene. VEGF (CYT-241), EGF (CYT-217), FGF-1 (CYT-362), PDGF-A (CYT-491), PDGF-B (CYT-492), and PDGF-D (CYT-155) were ordered from ProSpec Protein Specialists. The following antibodies used in the Western blot assay (all at 1:1,000 dilution) were ordered from Cell Signaling Technology: anti-GAPDH (catalog no. 2118S), anti-eIF4E1 (polyclonal; no. 9742), anti-eIF4G1 (no. 2498), and anti-eIF2α (no. 9722). DAPI (1:1,000 dilution in the immunofluorescence assay) was ordered from KPL. The following antibodies (all in 1:1,000 dilution) were ordered from Abcam: for the immunofluorescence assay, anti–γ-actin (γ-actin, monoclonal, ab123034) and anti–pan-cadherin (polyclonal, ab140338); for the Western blot assay, anti–MMP-3 (ab52915), anti-eIF4E2 (polyclonal, ab63062), anti-4EBP1(monoclonal, ab32130), anti–p-T37-4EBP1 (monoclonal, ab75767), anti-eIF1A (monoclonal, ab172623), anti-eIF5 (polyclonal, ab153730), and anti–PDGF-B (ab23914). The shRNA sets RHS4533-EG4314 (shRNA-*MMP3*, including five shRNAs) and RHS4533-EG1510 (shRNA-*CTSE*, including five shRNAs) were ordered from Dharmacon. The compound [*E*]-4EGI-1 isomer was ordered from SpeedChemical, and the purity and quality were confirmed by NMR. 4EGI-N(410E) was self-synthesized.

Transient Transfection. HMECs were cultured with MEGM at 37 °C in a humidified atmosphere of 5% CO_2. Plasmids of EGFP-hPMCA2z/b (no. 47584; Addgene) and/or mCherry–β-actin (no. 54967; Addgene) were cotransfected into HMECs using Lipofectamine 2000 (no. 11668027; Life Technologies) according to the manual. The cells were used for assays 2 d after transfection.

Development of Cytocapsulae and Cytocapsular Tubes. HMECs (with or without transfection) and BCSCs of the HMLER $(CD44^{high}/CD24^{low})^{FA}$ subpopulation were plated on a Matrigel matrix layer at the indicated cell densities (or at 5×10^2 cells per well in six-well-plates or 1.2×10^4 cells in 10-cm dishes, if not otherwise indicated) in MEGM medium. The 3D Matrigel layers (>40 μm in depth) were prepared by quickly adding cold Matrigel matrix (thawed in ice at 4 °C in a cold room overnight) to prechilled six-well plates (with or without cold micro cover glasses), followed by the addition of cold MEGM (4 °C) and incubation in the hood at room temperature (25 °C) for 5–25 min. Then the cells were implanted on the 3D Matrigel gel surface and cultured in a humidified incubator (37 °C, 5% CO_2). Cells in (or that had invaded into) the Matrigel gel in variable layers generated cytocapsulae and cytocapsular tubes. The developed cytocapsulae and cytocapsular tubes in various stages were used in this study.

Time-Lapse DIC Microscopy and Videos. Time-lapse DIC microscopy analyses of cytocapsula elongation and cell migration were performed using a Nikon Ti motorized inverted microscope and a digital Hamamatsu ORCA-ER cooled CCD camera with a 20× lens. The time-lapse microscope was equipped with DIC, phase contrast, and epi-fluorescence optics, a Prior ProScan III motorized stage and shutters, a perfect focus system, and an Okolab 37 °C, 5% CO_2 cage microscope incubator (Okolab). Images were taken every 30 s over the course of ∼10–36 h. All images were obtained using MetaMorph software. Tracks made by 2 h of cytocapsula elongation were obtained using MetaMorph and ImageJ software. Cytocapsula elongation velocities were also calculated using length and time measurements. Movies were prepared using the images collected via time-lapse and MetaMorph software (15 frames/s).

Imaging Acquisition. DIC and fluorescence images of fixed cells (with or without cytocapsulae) were taken with an 80i upright microscope and a digital Hamamatsu ORCA-ER cooled CCD camera with a 20× or 40× lens. The bright-field phase-contrast image was taken using a Nikon digital camera. The cytocapsula initiation ratio per high-performance field (HPF; 200×) and the number of elongated cytocapsulae per high-performance field were quantified. All images were obtained using MetaMorph image acquisition software and were analyzed with ImageJ software.

TEM. Matrigel matrix layers were prepared on plastic discs in six-well plates. HMEC cultures with cytocapsulae in Matrigel matrix (>40 μm in depth) were fixed with 1:1 mixtures of formaldehyde-glutaraldehyde-picric acid fixative (2.5% paraformaldehyde, 5.0% glutaraldehyde, 0.06% picric acid in 0.2 M cacodylate buffer):cell culture medium. The cells and cytocapsulae were then postfixed for 30 min in 1% osmium tetroxide (OsO_4)/1.5% potassium ferrocyanide ($KFeCN_6$), washed three times in water, and incubated in 1% aqueous uranyl acetate for 30 min followed by two washes in water and subsequent dehydration in grades of alcohol (50, 70, 95, and 2 × 100%; 5 min each) (1). Cells and cytocapsulae were infiltrated for 2 h to overnight in a 1:1 mixture of propylene oxide and TAAB Epon (Marivac Canada Inc.). The samples were subsequently embedded in TAAB Epon and polymerized at 60 °C for 48 h. Ultrathin sections (∼60 nm) were cut on a Reichert Ultracut S microtome, picked up on copper grids, stained with lead citrate, and examined in a JEOL 1200EX Transmission electron microscope or a Tecnai G2 Spirit BioTWIN microscope, and images were recorded with an AMT 2k CCD camera.

Animal Model and Immunohistochemistry Staining. A xenografted tumor model was used to study cytocapsular tubes in vivo. For the BCSC tumor cytocapsula examination, 1×10^5 BCSCs [HMLER $(CD44^{high}/CD24^{low})^{FA}$ subpopulation] were mixed with 100 μL of a 1:2 Matrigel:DMEM mixture (BD Biosciences). BCSCs/Matrigel/DMEM mixtures were s.c. injected into the mammary glands of 6-wk-old *NOD*/*SCID* female mice (the Jackson Laboratory) (five mice per group) (2–5). After the BCSC tumor developed to about 100 mm^3 in volume, the tumors were excised, fixed with HistoChoice MB fixative (Amresco) and were embedded in paraffin. For compound-treated BCSC tumors, 1×10^5 BCSCs were mixed with 100 μL of a 1:2 Matrigel/DMEM mixture (BD Biosciences). BCSCs/Matrigel/DMEM mixtures were s.c. injected into the mammary gland of *NOD*/*SCID* female mice (the Jackson Laboratory) (five mice per group). After the tumor formation (about 75 mm^3 in volume), DMSO (vehicle) or 75 mg/kg [*E*]-4EGI-1 was i.p. injected into the mice daily for 30 d. At the 30th day, mice were killed, and tumors were excised. Tumor tissue samples were used for immunohistochemistry staining. Sectioned BCSC tumor specimens were subjected to double immunohistochemistry staining with anti–pan-cadherin (1:200; ab140338; Abcam) and anti–γ-actin (1:200; ab123034; Abcam) primary antibodies and DAPI (1:1,000) for 4 h at 4 °C, followed by incubation with appropriate secondary antibodies for 1 h at 4 °C in a dark room. Fluorescence images were taken with a Nikon 80i upright microscope with a 20× or 40× lens. All images were obtained using MetaMorph image acquisition software and were analyzed with ImageJ software. Western blot assays were

performed. The mouse experiments were performed according to the policies of the Harvard Medical Animal Committee.

Total RNA Extraction and qPCR. TRIzol (Thermo Fisher Scientific) was used to extract total RNAs from HMECs and BCSCs (1.2×10^4 cells per 10-cm dish), with and without detectable cytocapsulae, at the indicated times. The samples used were those plated on Matrigel matrix layers (about 10 μm thick). Total RNAs were extracted as described in the manual. qPCR assays were performed using gene-specific primers (IDT Company), iQ SYBR Green Supermix (Bio-Rad), and 7900HT Fast Real-Time PCR according to the manufacturer's instructions. *GAPDH* was used as a control, and three independent experiments were performed. Data analyses and heatmap figures were calculated and prepared as previously described. Primer sequences are shown in Table S1.

Western Blotting. Using a radioimmunoprecipitation assay (RIPA) buffer [25 mM Tris·HCl (pH 7.6), 150 mM NaCl, 1% Nonidet P-40, 1% sodium deoxycholate, 0.1% SDS] and protease inhibitor (Roche), total proteins were extracted from the HMECs and BCSCs (1.2×10^4 cells per 10-cm dish), both with and without cytocapsulae, at the indicated times. The samples used were those implanted onto Matrigel matrix layers. The total proteins were electrophoresed through 10% or 12% SDS-polyacrylamide gels and were transferred onto polyvinylidene difluoride (PVDF) Immobilon-P membranes (EMD Millipore). PVDF membranes were probed with primary antibodies [anti-GAPDH (2118; Cell Signaling Technology), anti–MMP-3 (ab52915; Abcam), anti-eIF4E1 (9742; Cell Signaling Technology), anti-eIF4G1 (2498; Cell Signaling Technology), anti-eIF2α (9722; Cell Signaling Technology), anti-eIF4E2 (ab63062; Abcam), anti-4EBP1(ab32130; Abcam), anti–p-T37-4EBP1 (ab75767; Abcam), anti-eIF1A (ab172623; Abcam), anti-eIF5 (ab153730; Abcam), anti–PDGF-B (ab23914; Abcam), and anti–MMP-3 (ab52915; Abcam)] (all at 1:1,000 dilution) for 4 h at 4 °C followed by washing in 0.1% Tween 20 and Tris-buffered saline. Membranes were incubated with appropriate peroxidase-conjugated secondary antibodies at 25 °C for 1 h and were washed three times before signal detection. ECL Western blotting detection reagent was used for development.

Transient Gene Knockdown. The transient gene-knockdown effects of two shRNAs in each set were evaluated: RHS4533-EG4314 (shRNA-*MMP-3*, including five shRNAs) and RHS4533-EG1510 (shRNA-*CTSE*, including five shRNAs). The following two shRNAs in each set were used in the study: TRCN0000003339 [shRNA-*MMP-3* (1)] and TRCN0000003341 [shRNA-*MMP-3* (2)] for *MMP-3* knockdown and TRCN0000003666 [shRNA-*CTSE* (1)] and TRCN0000003668 [shRNA-*CTSE* (2)] for *CTSE* knockdown.

Quantification and Statistical Analysis. In all figures: no significance, ns, $P > 0.05$; $^{*}P < 0.05$; $^{**}P < 0.01$; $^{***}P < 0.001$. The statistical methods used for comparisons are indicated in the relevant figure legends and in the sections below. The diameters, widths, and lengths of cytocapsulae and cytocapsular tubes were measured with ImageJ. The time of individual cytocapsulae and cytocapsular tubes was counted from cytocapsula generation to acellular cytocapsula (or cytocapsular tube) decomposition. For lifetime of cytocapsulae and cytocapsular tubes assays (Figs. 1 *F* and *M* and 4*H* and Fig. S2*E*), at least 20 cytocapsulae or cytocapsular tubes were measured per condition, and two-tailed Student's test was used to determine statistical significance. For the ratio of cytocapsula diameter/width to cell diameter assay (Fig. 1*G*), at least 20 cytocapsulae with intraluminal cells were counted per condition, and two-tailed Student's test was used to determine statistical significance. The graphs in Fig. 1 *H* and *M* plot the mean ± SD from three independent experiments, and the two-tailed Student's test was used to determine statistical significance. Densitometric measurements were carried out using Image Studio Lite version 3.1 (Li-COR Biosciences). In Figs. 5*D* and 6 *A* and *F*, at least three independent experiments were performed, and a representative image is shown with the relative densities of bands. Real-time transcription measurements of 34 genes during cytocapsular tube development were carried out with qPCR. Three independent experiments were performed. The average relative log-twofold change is shown in the heat maps. Cells migrating in the cytocapsular tubes were imaged with a time-lapse DIC microscope, and the migration distances were measured with ImageJ. The cell migration speeds were calculated. In Fig. 4*C*, the graph plots the mean ± SD of at least three single cells per condition and three individual cells (streaming) in chains (one cell per chain). Single cells generating elongated cytocapsular tubes were imaged with a time-lapse DIC microscope, and the elongated lengths were measured with ImageJ. The cytocapsular tube elongation speeds were calculated. In Fig. 5*H*, at least 15 cytocapsular tubes were tracked per condition, and two-tailed Student's test was used to determine statistical significance.

1. Weninger W, Biro M, Jain R (2014) Leukocyte migration in the interstitial space of non-lymphoid organs. *Nat Rev Immunol* 14:232–246.
2. Yi T, et al. (2014) Quantitative phosphoproteomic analysis reveals system-wide signaling pathways downstream of SDF-1/CXCR4 in breast cancer stem cells. *Proc Natl Acad Sci USA* 111:E2182–E2190.
3. Scheel C, et al. (2011) Paracrine and autocrine signals induce and maintain mesenchymal and stem cell states in the breast. *Cell* 145:926–940.
4. Tam WL, et al. (2013) Protein kinase C α is a central signaling node and therapeutic target for breast cancer stem cells. *Cancer Cell* 24:347–364.
5. Song SJ, et al. (2013) MicroRNA-antagonism regulates breast cancer stemness and metastasis via TET-family-dependent chromatin remodeling. *Cell* 154:311–324.

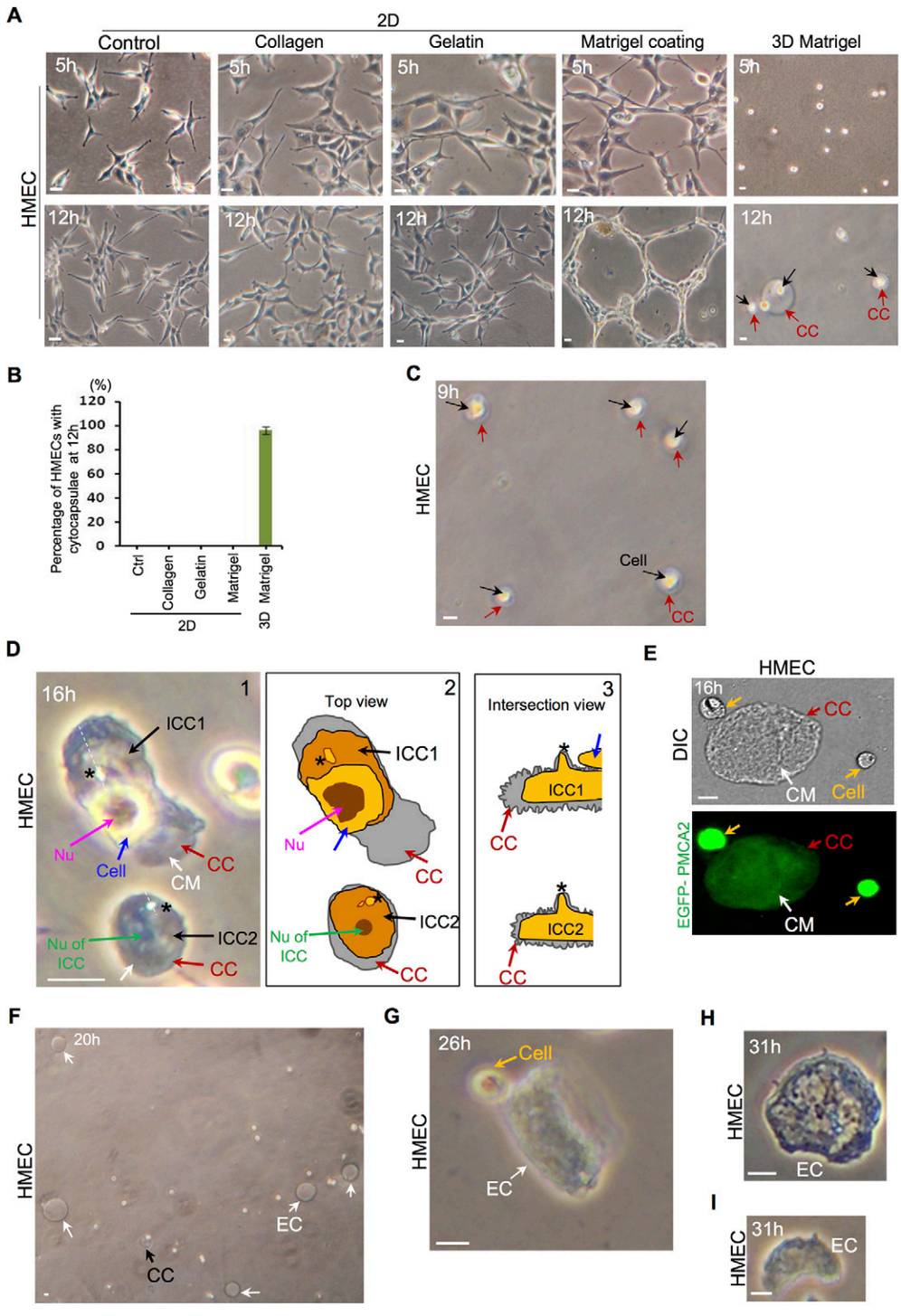

Fig. S1. Generation and lifecycle of cytocapsulae. (*A*) Phenotypic analyses of HMECs under multiple 2D conditions and in 3D Matrigel environments. Under 2D conditions and on rigid surfaces, HMECs constantly present flat, irregular morphologies. At 12 h postimplantation on 2D Matrigel coating, HMECs polarize, aggregate, and form tube-like structures. In 3D Matrigel, at 5 h, HMECs exhibit a small, stringent, spherical morphology, and at 12 h single spherical HMECs (black arrows) generate extracellular cytocapsulae (CC, red arrows) in variable sizes. (*B*) Quantitation of data from *A*; $n = 3$. (*C*) Cytocapsula initiation. Single spherical HMECs engender small, round extracellular cytocapsulae (CC, red arrows) enclosing the cells (black arrows). (*D*) Shrinkage of cytocapsulae. (*1*) Shrunken cytocapsular membranes envelope the two intracytocapsular cells (ICC1, and ICC2) and dim the golden color of the intracytocapsular cells. The small protrusions of the intraluminal cells stretch and unfold the local folded cytocapsular membrane (CM) and present the cellular color (golden in this image, indicated by a black asterisk). A cell (blue arrow) migrates onto and resides on the cytocapsula of ICC1 and displays golden color in the image. (*2* and *3*) Schematic diagrams of the top view (*2*) and an intersection view (*3*). The nucleus of ICC2 (Nu, green arrow) and the nucleus (Nu, purple arrow) of the cell (blue arrow) migrating onto the cytocapsula of ICC1 are shown. (*E*) DIC and fluorescence microscope examination of cytocapsular membranes. HMECs were transfected with EGFP–PMCA2 plasmid. EGFP–PMCA2 is distributed through the cell plasma membranes and cytocapsular membranes (CM, white arrows) of a large cytocapsula (CC, red arrows), whose membranes are slightly folded. (*F*) Ecellularization of cytocapsulae (CC, black arrow). Multiple round, ecellulated cytocapsulae (EC, white arrows) are shown. The membranes of acellular cytocapsulae are taut with no visible shrinkage. (*G*) A deflated, shrunken, short, tube-shaped, ecellulated cytocapsula (EC) with its repulsed cell. (*H*) An ecellulated cytocapsula (EC) in a deflated, concave disc morphology with the degraded membrane in the center area. (*I*) An ecellulated cytocapsula (EC) in severe decomposition, with the remaining part in a deflated convex–concave morphology. (Scale bars: 10 μm.)

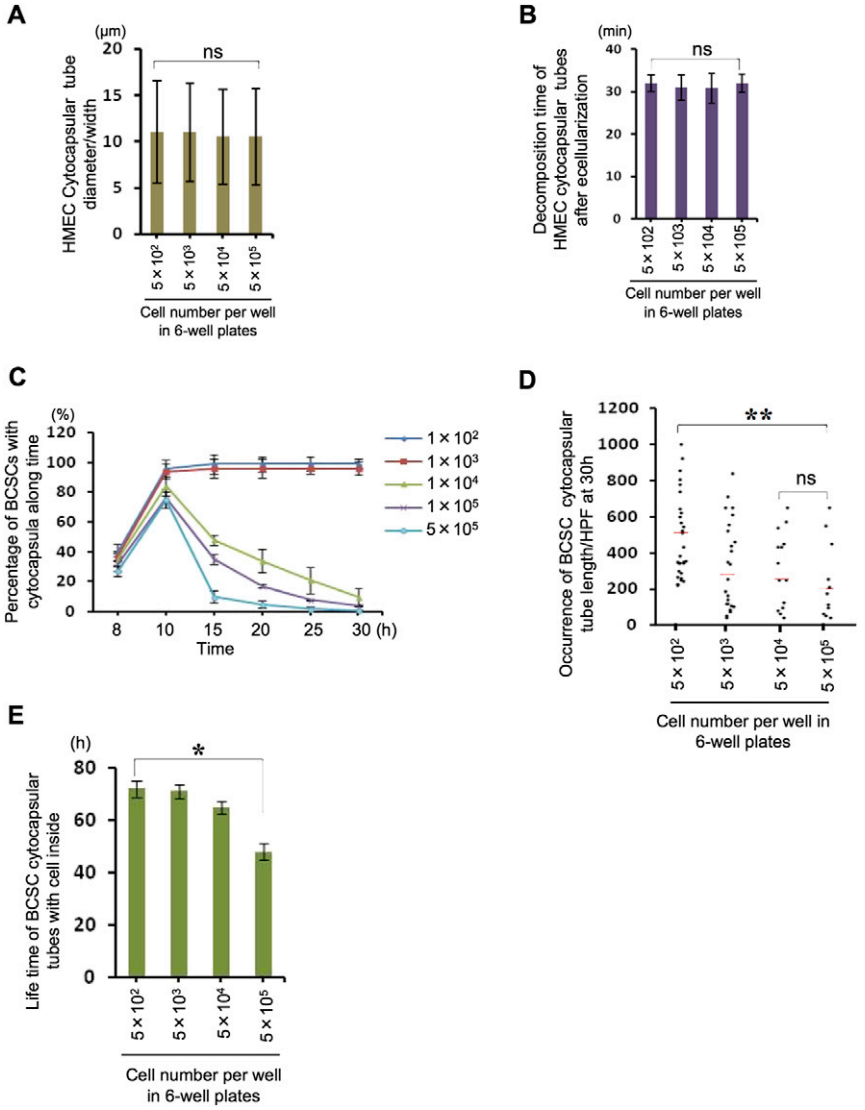

Fig. S2. Characterization of cytocapsulae and cytocapsular tubes. (*A*) Quantitation of HMEC cytocapsula diameter; $n = 3$. (*B*) Quantitation of HMEC cytocapsula decomposition after ecellularization; $n = 3$. (*C*) Quantitation of BCSC cytocapsula generation; $n = 3$. (*D*) Occurrence of BCSCs with cytocapsular tubes and their lengths. The scatterplot compares cytocapsular tube occurrence and length per condition. Red lines indicate the mean; $n = 2$. (*E*) Quantitation of BCSC cytocapsular tube durance; $n = 3$. ns, $P > 0.05$; $*P < 0.05$; $**P < 0.01$.

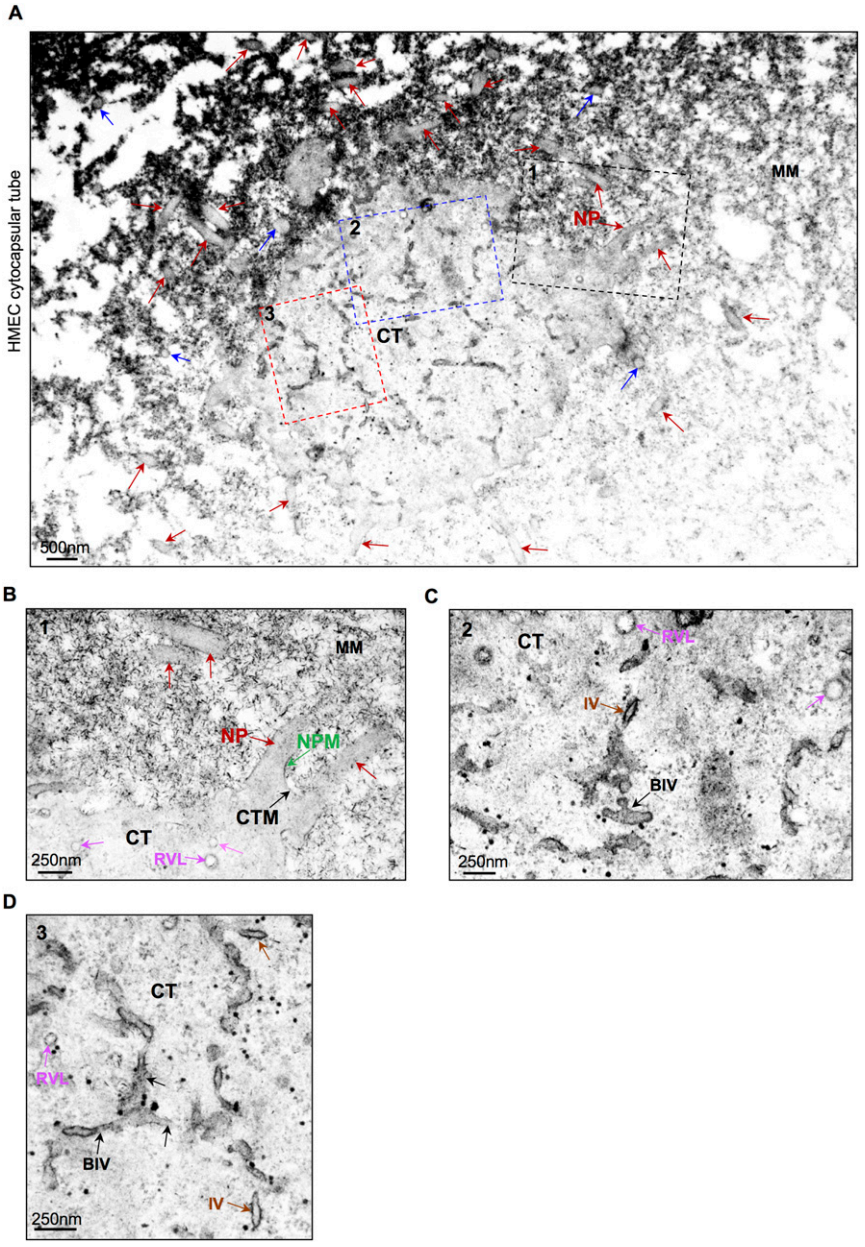

Fig. S3. Ultrastructure of HMEC cytocapsular tubes. (*A*) A TEM image of the transverse section of an elongated HMEC cytocapsular tube. The cytocapsular tube (CT), cytocapsular tube nanoprotrusion (NP; longitudinal section, red arrows; transverse section, blue arrows), and Matrigel matrix (MM) are shown. The three framed areas (1–3) are enlarged and shown in *B*–*D*, respectively. (*B*) The membranes of cytocapsular tube protrude and form nanoprotrusions (NP). The cytocapsular tube (CT) membrane (CTM; black arrow) and connected nanoprotrusion membranes (NPM; green arrow) are shown. A round vesicle with low electron density (RVL; purple arrows) and longitudinal sectioned nanoprotrusions (NP; red arrows) are shown. (*C*) In the cytocapsular tube lumen, a branched irregular vesicle with branches (BIV; black arrow), an irregular vesicle with no branch (IV; dark brown arrow), and a round vesicle with low electron density (RVL; purple arrows) are shown. (*D*) Isolated small membranous vesicles, including a branched irregular vesicle with middle branches (BIV; black arrow), an irregular vesicle with no branch (IV; dark brown arrow), and a round vesicle with low electron density (RVL; purple arrows) are shown.

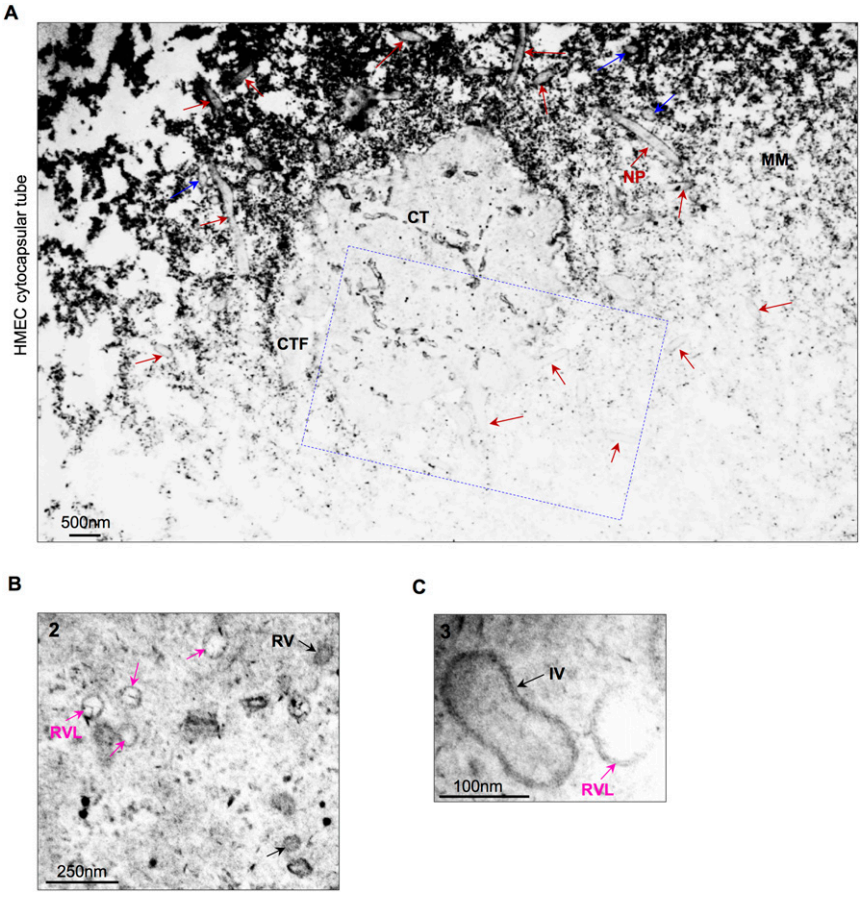

Fig. S4. Ultrastructure of 3D HMEC cytocapsular tubes. (*A*) TEM image of the cross-sectioned specimen next to the specimen in Fig. S3*A*. The framed area is enlarged and shown in Fig. 2*A*. A cytocapsular tube (CT), a cytocapsular tube fold (CTF), and a cytocapsular tube nanoprotrusion (NP; longitudinal section, red arrows; transverse section, blue arrows) are shown. (*B*) Enlargement of area 2 in Fig. 2*A*. Small, round vesicles with low electron density (RVL; purple arrows) and a round vesicle with dense electron density (RV; black arrow) are shown. (*C*) Enlargement of area 3 in Fig. 2*A*. An irregular vesicle (IV; black arrow) and a round vesicle with low electron density (RVL; purple arrow) are shown.

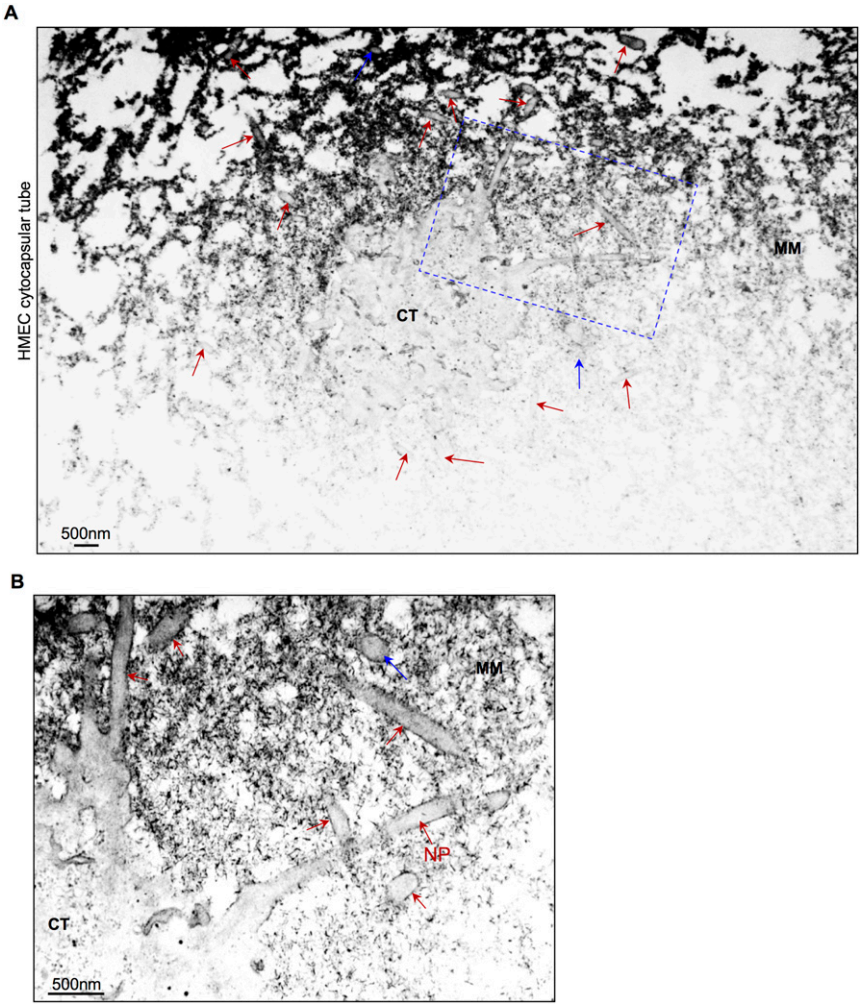

Fig. S5. Characterization of the ultrastructure of 3D HMEC cytocapsular tubes. (*A*) TEM image of the cross-sectioned specimen next to the specimen in Fig. S4*A*. A cytocapsular tube (CT) and a cytocapsular tube nanoprotrusion (NP; longitudinal section, red arrows; transverse section, blue arrows) are shown. The framed area is enlarged and shown in *B*. (*B*) Long cytocapsular tube nanoprotrusions (NP; longitudinal section, red arrows; transverse section, blue arrows) crossing each other in different layers are shown.

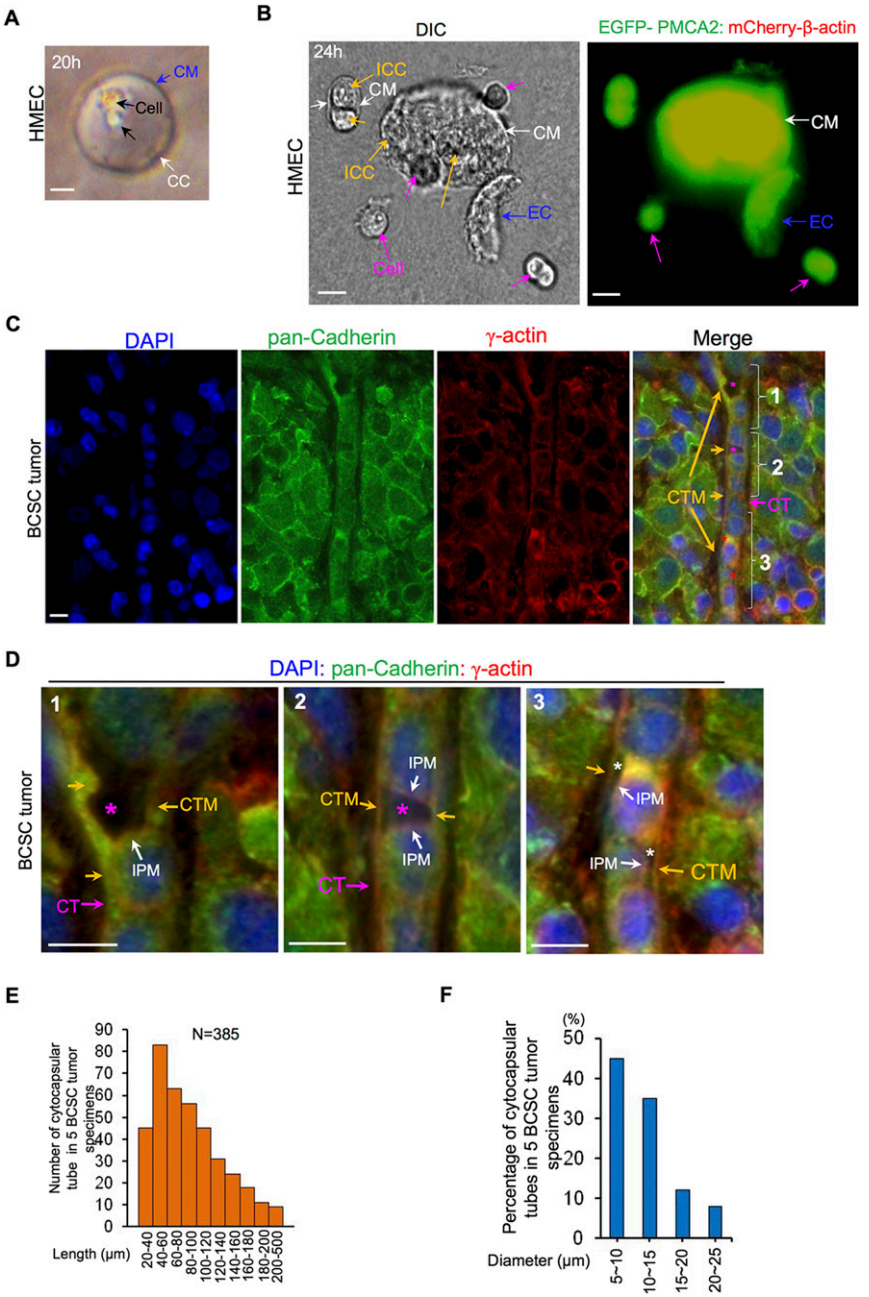

Fig. S6. Cell entry and cells migrating in long cytocapsular tubes in tissues in vivo. (*A*) An HMEC enters a large, round cytocapsula of another cell, resulting in a single cytocapsula (CC) harboring two intraluminal cells. CM, cytocapsular membrane. (*B*) DIC and fluorescence microscope analyses of alloentry of cytocapsulae. In the upper left of the DIC image, an oval cytocapsula contains two intracytocapsular cells (ICC; orange arrows). In the center, a large oval cytocapsula harbors at least two intracytocapsular cells whose outlines are discernible in the DIC image. All the intraluminal cells are masked by the extracellular cytocapsular membranes (CM; white arrows) and are indiscernible in the fluorescence image. The cells outside the cytocapsula (purple arrows) and a shrunken, ecellulated cytocapsula (EC; blue arrow) are shown. (Scale bars: 10 μm.) (*C*) Immunohistochemistry analysis of cell migration in cytocapsular tubes with BCSC tumors. BCSC tumor section specimens (5 μm in depth) were immunostained with DAPI, anti–pan-cadherin, and anti–γ-actin antibodies. Multiple nucleated cancer cells migrate in the long, membranous cytocapsular tubes in compacted tumor tissue environments. The long, seamless, nonnucleus cytocapsular tube membranes (CTM, orange arrows) are shown. The γ-actin signals are distributed along the cytocapsular tube membranes but not in the lumens (purple asterisks). The distribution of γ-actin signals overlaps that of pan-cadherin signals along the cytocapsular tube membranes. The three fragments of a cytocapsular tube are enlarged and shown in *D*. (*1*) In the large cytocapsular tube lumen (purple asterisk), there is no γ-actin signal. (*2*) A luminal gap with no γ-actin signal between two intraluminal cells is shown. (*3*) Two small luminal gaps (white asterisks) between cytocapsular tube membrane and intraluminal cell plasma membrane are shown. The cytocapsular tube (CT), membrane (CTM; orange arrows), and intraluminal cell plasma membrane (IPM) are shown. (Scale bars: 10 μm.) (*E*) Quantitation of cytocapsular tube lengths in *C*. (*F*) Quantitation of cytocapsular tube diameters in *C*.

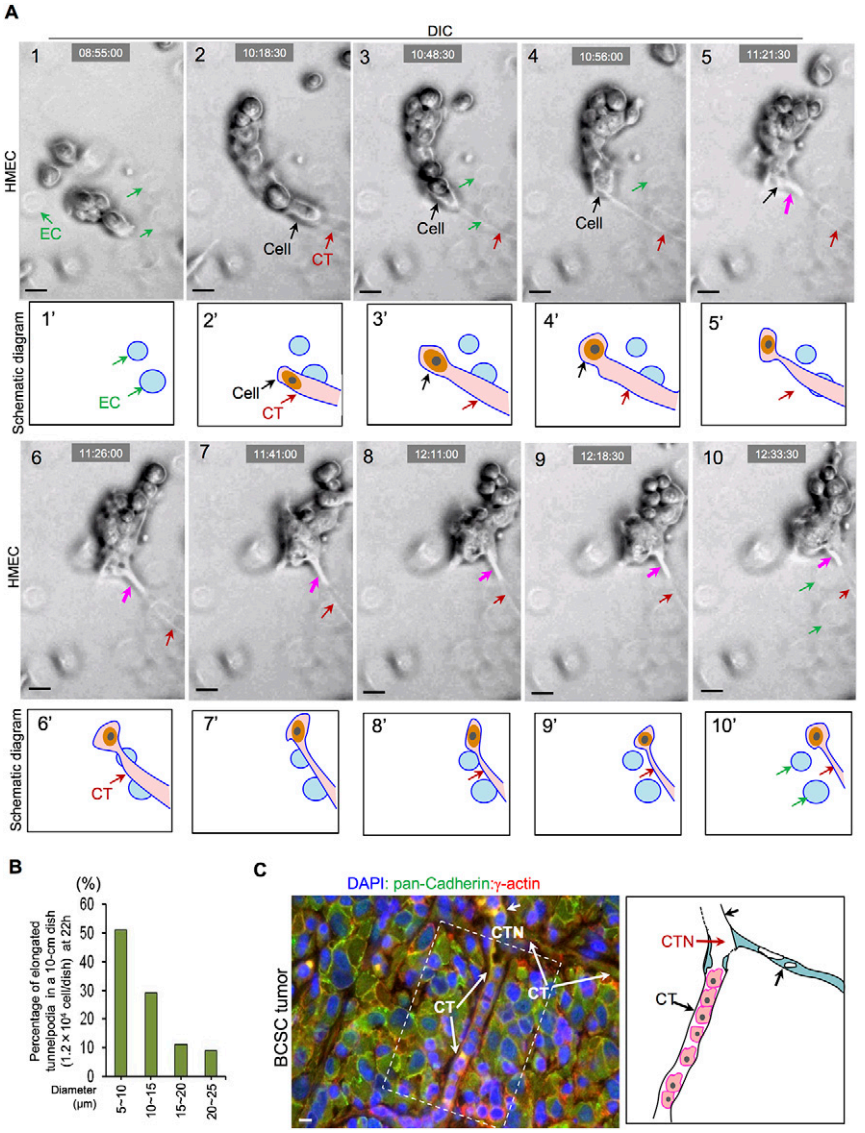

Fig. S7. Cytocapsular tube elongation and network formation. (*A*) Real-time analysis of cytocapsular tube generation and elongation with a time-lapse DIC microscope. (*1*) There are several small, round ecellulated cytocapsulae (EC; white ring-shaped in the image, green arrows) in the 3D Matrigel. Multiple cells migrate, aggregate, and form a short cell chain. (*2*) Multiple cells migrate in streaming. A single cell (black arrow) in its cytocapsular tube (CT; red arrow) follows the moving cell chain. The labeled single cell advances, pushes, deforms, and generates elongated membranes and engenders an elongated cytocapsular tube. (*3*) The labeled cell has generated an elongated cytocapsular tube, which lies in the Matrigel and cannot automatically move or change its direction. (*4*) The cell continues to advance and has generated a long (~40 μm in length), large (~8 μm in diameter/width) cytocapsular tube (CT; red arrow). The cytocapsular tube continues to lie in the Matrigel and cannot automatically move, or change its direction. The cell begins to change the direction of migration. (*5*) The cell changes the direction of migration and drags its long cytocapsular tube, forming a contracted and condensed membrane fragment (purple arrow). (*6–10*) The cell migrates and drags its contracted cytocapsular tube across ECM surfaces and multiple small, round acellular cytocapsulae without breakage, interruption, or interception. (Scale bars: 10 μm.) Schematic diagrams (*1′–10′*) of each image are shown. Ecellulated cytocapsula (EC; green arrows), cell (black arrow), and cytocapsular tube (CT; red arrow) are shown. (*B*) Quantitation of cytocapsular tube diameters in *A*. (*C*, *Left*) Validation of cytocapsular tube networks in vivo. Cytocapsular tubes (CT; white arrows) interconnect and form networks via cytocapsular tube connection nodes (CTN). Multiple cells migrate in the cytocapsular tube networks. The framed area is enlarged and shown in *A*. (Scale bar: 10 μm.) (*Right*) Schematic diagram of the cytocapsular tube network shown at the left.

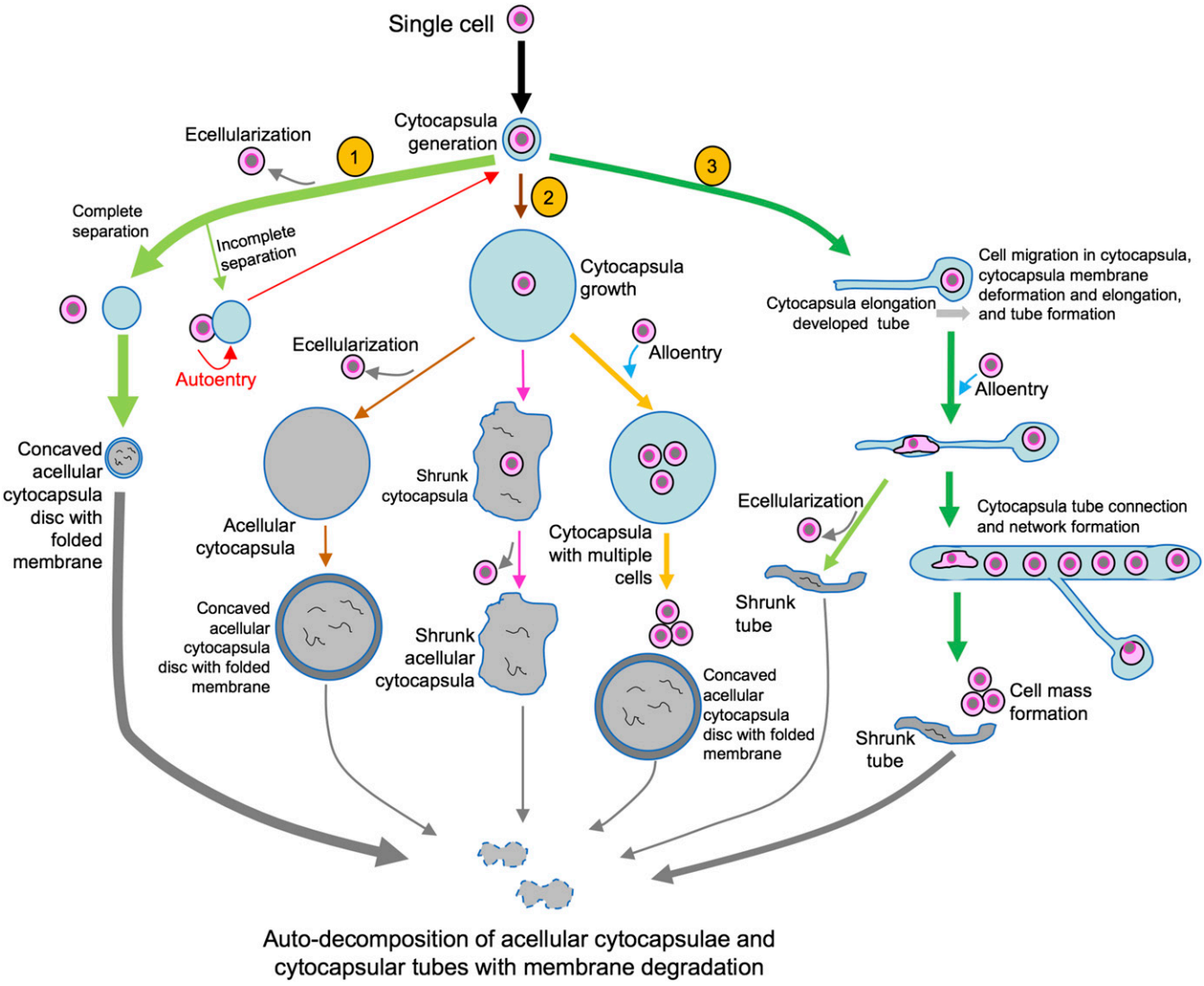

Fig. S8. Schematic diagram of the cytocapsula and cytocapsular tube lifecycle. Initially, single mammalian cells generate small, round, extracellular membranous cytocapsulae enclosing the cell. Subsequently, cytocapsulae proceed through multiple distinct development stages. (*1*) Cytocapsulae proceed through ecellularization with complete separation of the acellular cytocapsulae and expulsed cells. In ecellularization with incomplete separation, the evicted cells have connections to their acellular cytocapsulae and can reenter their acellular cytocapsulae via autoentry and reform closed cytocapsulae with cells in the lumens. (*2*) Cytocapsulae grow and form large (100–250 μm in diameter/major axis), round or oval cytocapsulae. The large cytocapsulae can shrink slightly and form shrunken cytocapsulae enclosing the intraluminal cells. On the other hand, other cells can enter single large cytocapsulae that already contain cells, resulting in single cytocapsulae harboring multiple cells. Ecellularization of these large cytocapsulae generates large acellular cytocapsulae, which shrink, deflate, and form large, deflated, concave discs (or irregular morphologies). (*3*) Cells migrate in their cytocapsulae, deform cytocapsular membranes, and generate elongated cytocapsular tubes. Alloentry permits multiple cells to enter and migrate in cytocapsular tubes. The migration of a single cell or multiple cells in the homogeneous and membrane-enclosed cytocapsular tubes is faster than migration in the heterogeneous environments composed of heterogeneous ECM and other cells. Cytocapsular tubes interconnect and form branched, seamless, membranous tube networks, providing tubular web systems for directed 3D cell transportation in diverse directions. Ecellularization generates acellular cytocapsular tubes. All the acellular cytocapsulae and cytocapsular tubes undergo rapid self-decomposition.

Table S1. Primer sequences of 34 human proteases used in qPCR analyses

Protease	Gene name	Sense	Antisense
ADAM8	*ADAM8*	CACAACTTCACCCTCCACCT	GAGTCCGGGTACCCCTCTAC
ADAM9	*ADAM9*	GCATTTGTGGGAACAGTGTG	GCTCTTTGCTCCACAGGAAC
ADAMTS1	*ADAMTS1*	TAGGACAGCCCACAGGAACT	CCCTTCTGTTCATCGTGGAT
ADAMTS13	*ADAMTS13*	ATCAACCCTGAGGACGACAC	TAATGAGGCAGCTCCAGGTT
Cathepsin A	*CTSA*	CTGCTGCTGCTAGTGTCCTG	CTGGGACTCCACAAACCAGT
Cathepsin B	*CTSB*	GCTATCCTGCTGAAGCTTGG	CTGTTTGTAGGTCGGGCTGT
Cathepsin C	*CTSC*	TTGTTTCACCGGAAAGAAGG	GTGGCCACCACTTCTCCTAA
Cathepsin D	*CTSD*	CTGCACAAGTTCACGTCCAT	ACTGGGCGTCCATGTAGTTC
Cathepsin E	*CTSE*	ATCCAGTTCACCGAGTCCTG	GTACACAGAGGGGACCCAGA
Cathepsin L	*CTSL*	AGGGAAGGGAAACACAGCTT	AAGCCCAACAAGAACCACAC
Cathepsin S	*CTSS*	TCATACGATCTGGGCATGAA	AGCAAGCACCACAAGAACCT
Cathepsin V	*CTSV*	TGACGCCAGTGAAGAATCAG	CTAGCCATGAAGCCACCATT
Cathepsin X/Z/P	*CTSZ*	GCAATGTGGATGGTGTCAAC	GTAGTCCCACACGGACAGGT
DPPIV	*DPP4*	CATGGGCAACACAAGAAAGA	TCTTCCAACCCAGCCAGTAG
Kallikrein 3	*KLK3*	TCATCCTGTCTCGGATTGTG	ATATCGTAGAGCGGGTGTGG
Kallikrein 5	*KLK5*	GTCTCCTCTCATTGTCCCTCTG	CGCAGAACATGGTGTCATCTAT
Kallikrein 6	*KLK6*	AAGAAGCTGATGGTGGTGCT	CCCACAGTGGATGGATAAGG
Kallikrein 7	*KLK7*	TCAAGGCCTCGAAGTCATTC	CCGGAGACAGTACAGGTGGT
Kallikrein 10	*KLK10*	GTCCTGGTGGACCAGAGTTG	CCAGCTTCAGCAACATGAGA
Kallikrein 11	*KLK11*	CATCATGCTGGTGAAGATGG	GGTGCTCAATGATGGTGATG
Kallikrein 13	*KLK13*	CAAAACTCTACAATGTGCCAACA	CGATGCCATACAGTGTTCTGTTA
MMP-1	*MMP1*	GGTCTCTGAGGGTCAAGCAG	AGTTCATGAGCTGCAACACG
MMP-2	*MMP2*	AGTGGATGATGCCTTTGCTC	GAGTCCGTCCTTACCGTCAA
MMP-3	*MMP3*	GCAGTTTGCTCAGCCTATCC	GAGTGTCGGAGTCCAGCTTC
MMP-7	*MMP7*	GAGTGCCAGATGTTGCAGAA	GCCAATCATGATGTCAGCAG
MMP-8	*MMP8*	AATGGAATCCTTGCTCATGC	GTTGCTGGTTTCCCTGAAAG
MMP-9	*MMP9*	GAGACCGGTGAGCTGGATAG	TACACGCGAGTGAAGGTGAG
MMP-12	*MMP12*	ACACCTGACATGAACCGTGA	ATGGGCTAGGATTCCACCTT
MMP-13	*MMP13*	TTGAGCTGGACTCATTGTCG	GGAGCCTCTCAGTCATGGAG
Neprilysin	*MME*	ATATGGGTGGCCAGTAGCAA	CCAAGTCGAGGTTGGTCAAT
Presenilin-1	*PSEN1*	AATAGAGAACGGCAGGAGCA	CACAGGGACAAAGAGCATGA
Proprotein convertase 9	*PCSK9*	ACCCTCATAGGCCTGGAGTT	GAGTAGAGGCAGGCATCGTC
Proteinase 3	*PRTN3*	ACGACGTTCTCCTCATCCAG	GTGACCACGGTGACATTGAG
uPA/urokinase	*PLAU*	ATTCACCACCATCGAGAACC	CTTGAGCGACCCAGGTAGAC

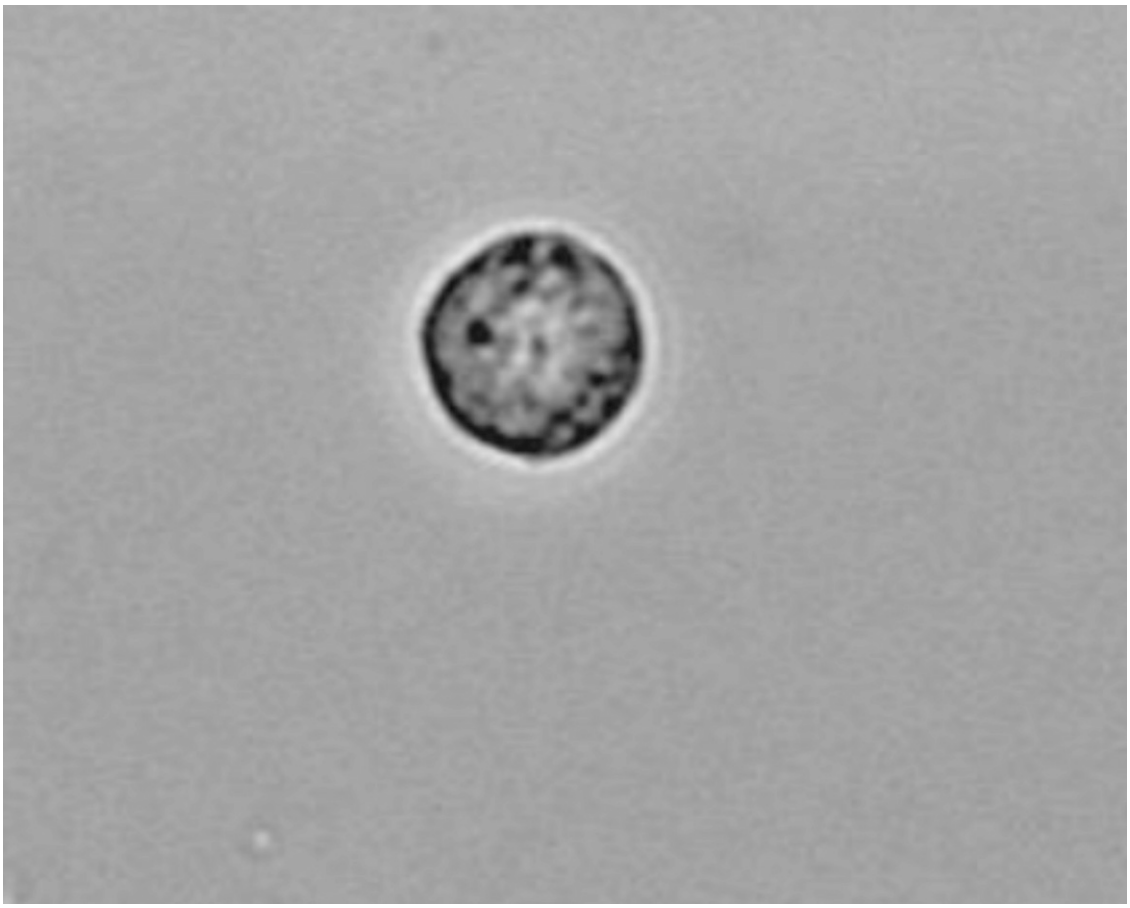

Movie S1. The cytocapsula processes ecellularization with incomplete separation. The evicted cell actively and repeatedly generates and retracts multiple long or short pseudopodia protrusions. The deformed acellular cytocapsula remodels and forms a round morphology. The cell reenters the acellular cytocapsula and reunites into a cytocapsula with a single cell inside. Representative DIC images are shown in Fig. 3*C*.

Movie S1

Movie S2. Single HMECs enter the long cytocapsular tubes of other cells in five successive steps: (*i*) initiation; (*ii*) half entry; (*iii*) majority entry; (*iv*) complete entry and tube membrane remodeling and reclosing; and (*v*) cell migration in cytocapsular tubes of other cells. Representative DIC images are shown in Fig. 4*A*.

Movie S2

Movie S3. Single HMECs advance in their cytocapsulae, deform cytocapsular membranes, and generate elongated, extracellular, seamless, membranous cytocapsular tubes. When the cell changes the direction of migration, the cell contracts its cytocapsular tube, forming a contracted, membrane-condensed fragment. The cell drags its cytocapsular tube across the ECM surfaces without tubular breakage, interruption, or interception. Representative DIC images are shown in Fig. S5*A*.

Movie S3

Other Supporting Information Files

Dataset S1 (PDF)